High Flux Thin Film Nanocomposite Membranes Based on Metal–Organic Frameworks for Organic Solvent Nanofiltration

Sara Sorribas,[†,‡] Patricia Gorgojo,[†,§] Carlos Téllez,[‡] Joaquín Coronas,*[,‡] and Andrew G. Livingston*[,†]

[†]Department of Chemical Engineering, Imperial College, Exhibition Road, South Kensington Campus, London SW7 2AZ, U.K.

[‡]Chemical and Environmental Engineering Department and Instituto de Nanociencia de Aragón (INA), Universidad de Zaragoza, 50018 Zaragoza, Spain

S Supporting Information

ABSTRACT: Thin-film nanocomposite membranes containing a range of 50−150 nm metal−organic framework (MOF) nanoparticles [ZIF-8, MIL-53(Al), NH_2-MIL-53(Al) and MIL-101(Cr)] in a polyamide (PA) thin film layer were synthesized via in situ interfacial polymerization on top of cross-linked polyimide porous supports. MOF nanoparticles were homogeneously dispersed in the organic phase containing trimesoyl chloride prior to the interfacial reaction, and their subsequent presence in the PA layer formed was inferred by a combination of contact angle measurements, FT-IR spectroscopy, SEM, EDX, XPS, and TEM. Membrane performance in organic solvent nanofiltration was evaluated on the basis of methanol (MeOH) and tetrahydrofuran (THF) permeances and rejection of styrene oligomers (PS). The effect of different post-treatments and MOF loadings on the membrane performance was also investigated. MeOH and THF permeance increased when MOFs were embedded into the PA layer, whereas the rejection remained higher than 90% (molecular weight cutoff of less than 232 and 295 g·mol^{-1} for MeOH and THF, respectively) in all membranes. Moreover, permeance enhancement increased with increasing pore size and porosity of the MOF used as filler. The incorporation of nanosized MIL-101(Cr), with the largest pore size of 3.4 nm, led to an exceptional increase in permeance, from 1.5 to 3.9 and from 1.7 to 11.1 L·m^{-2}·h^{-1}·bar^{-1} for MeOH/PS and THF/PS, respectively.
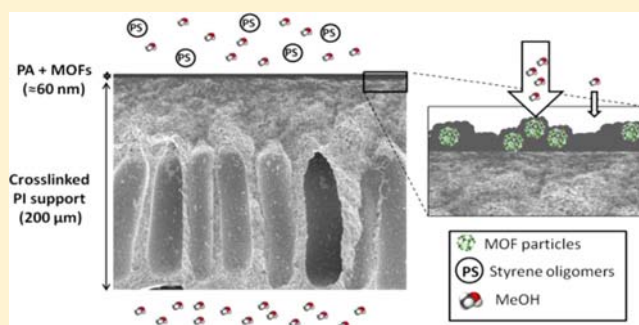
INTRODUCTION

Organic solvent nanofiltration (OSN) is an emerging technology for molecular separation and purification in organic solvents that economically and efficiently separates molecules in the 200−1000 g·mol^{-1} range by simply applying a pressure gradient across a membrane.[1] Since OSN membranes are commercially available and can be "tailor-made" for specific purposes, they are used in many applications related to petrochemistry, food, biotechnology, and pharmaceutical industries. The main challenge for OSN membranes is the development of materials that are stable in a wide range of organic solvents. In addition, they must show high and reproducible performance over the long-term, which combines elevated solvent permeances with acceptable rejections.

Many of the OSN membranes developed to date are integrally skinned asymmetric membranes made of polyimides,[2] but these are limited in terms of flux for some organic solvents. Thin film composite (TFC) membranes, first developed by Cadotte via interfacial polymerization (IP) in the 1970s,[3] can also be produced for OSN applications. They consist of an ultrathin separating barrier layer prepared via IP on top of a porous support. Using this kind of membrane the ultrathin barrier layer and the porous support can independently be optimized to meet the requirements for target application.

Polyimides (PI) have been used for the fabrication of membranes for solvent resistant nanofiltration and ultra-filtration.[4,5] PI are stable in a wide range of organic solvents and have high temperature durability and good mechanical properties when cross-linked.[6−8]

The copolyimide P84 has been reported to be stable in organic solvents including polar aprotic solvents such as dichloromethane, tetrahydrofuran, N-methylpyrrolidone, and dimethylformamide (DMF) after chemical cross-linking.[4] When this polyimide is cross-linked and used as a support for TFC membranes, it permits the post-treatment of the TFC membranes with aggressive polar aprotic solvents (DMF or dimethyl sulfoxide) which modify the surface, removing small molecular fragments and generating a more open structure, thus enhancing permeation fluxes without sacrificing rejection.[12]

Interfacial polymerization of thin film nanocomposite (TFN) membranes was first developed by Jeong et al.[13] They are usually formed by embedding molecular sieve nanoparticles throughout a polyamide (PA) thin film layer of an interfacially polymerized composite membrane. In reverse osmosis
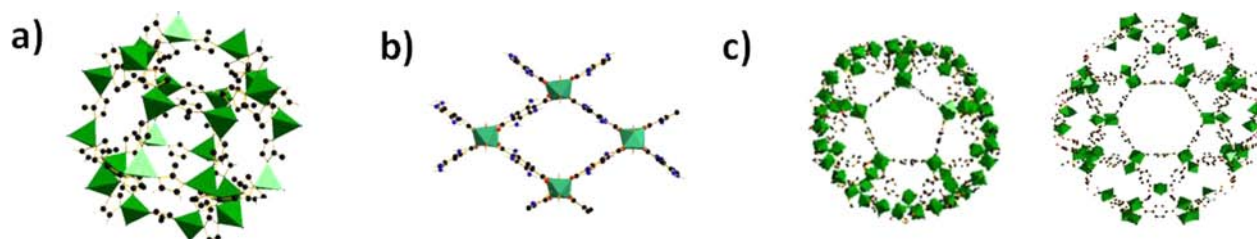
Figure 1. (a) Building blocks of ZIF-8, with the ZnN_4 tetrahedra in green; (b) pore system in NH_2-MIL-53(Al), with the AlO_6 octahedra in green; and (c) building blocks for MIL-101(Cr) with the trimers of Cr octahedra in green. The zeotype architecture of MIL-101 displays mesoporous cages with diameters of 29 and 34 Å, featuring 12 Å pentagonal and 16 Å hexagonal openings. Oxygen, nitrogen, and carbon atoms are in red, blue, and black, respectively. These structures were made with Diamond 3.2. using the corresponding CIF files.[9−11]

membranes, nanoparticles of zeolite NaA, a hydrophilic and negatively charged three-dimensional molecular sieve pore network, were dispersed in the PA thin film by interfacial polymerization. This dramatically improved permeance and interfacial properties when compared to similarly formed pure PA thin films.[13] MCM-41 silica nanoparticles were also introduced into the TFN membrane for water purification,[14,15] showing an enhanced performance in comparison with the nonmodified membrane. PA-TiO_2 nanocomposite membranes were also reported by Lee et al.[16] and had a rejection value for $MgSO_4$ of around 95% and a water permeation flux of 9.1 L·$m^{−2}$·$h^{−1}$ at 0.6 MPa.

Metal−organic frameworks (MOFs) are hybrid inorganic−organic solid compounds with zeolite-like structures whose properties overcome the limitations of zeolites in terms of materials chemistry.[17] MOFs are being studied extensively owing to their exceptionally high surface area, controlled porosity, functionalizable pore walls, affinity for certain molecules, tunable chemical composition, and flexible structure. The use of MOFs as fillers offers potential advantages over other nanostructured porous materials such as zeolites. Due to the organic linkers present in their structure, MOFs have better affinity for the polymeric chains than inorganic fillers; therefore, it is easier to control MOF−polymer interface interactions, and nonselective voids between the phases can be avoided. In addition, by choosing the appropriate ligands or using postsynthetic functionalization, MOFs' flexibility in chemical design and in pore size and shape may facilitate interactions with the polymer and adjust their cavities to a particular application.[18] Unlike traditional inorganic zeolites with "rigid" frameworks, MOFs are in general structurally flexible.[19] As a result, their framework structure can be adapted according to the guest molecules, and high selectivity for adsorption and encapsulation can be achieved. For these reasons, the combination of MOF crystals with a polymer to form a composite or mixed-matrix membrane (MMM) for gas separation applications has been widely studied.[20] However, studies of liquid separation lag behind; it is only recently that the first studies for pervaporation[21,22] and nanofiltration[23] have been carried out. The incorporation of modified MOFs [HKUST-1, MIL-47, MIL-53(Al) and ZIF-8] in 30−35 μm polydimethylsiloxane (PDMS) membranes on a PI support has been reported for the separation of Rose Bengal from 2-propanol.[23] In that work, although the membranes had similar permeance values, the retention of Rose Bengal by the MMMs was significantly higher than that of unfilled PDMS membranes, due to the reduction of polymer swelling and the size exclusion of the filler.

We report here, for the first time, the use of MOFs as fillers in TFN membranes. The preparation of TFN membranes for OSN by embedding nanoparticles of hydrophilic and hydrophobic MOFs is explored. ZIF-8, MIL-53(Al), NH_2-MIL-53(Al), and MIL-101(Cr) (see Figure 1) were successfully incorporated into the polyamide layer via IP. Moreover, TFN membranes previously reported were used exclusively for desalination applications, and this is, to the best of our knowledge, the first study in which TFN membranes have been used for OSN. The chosen support is cross-linked PI P84, whose synthesis was first reported by our group.[4,12] The compatibility between polymer and filler in the resulting MMMs was enhanced due to the presence of organic ligands of MOFs. To best match the characteristic thickness of the TFN membrane, which is between 100 and 300 nm,[24] the particle size of the MOFs was controlled to be around 50−150 nm.

■ EXPERIMENTAL SECTION

Syntheses of MOFs. The synthesis of ZIF-8 was carried out as previously reported.[25] Activated ZIF-8 nanocrystals with high porosity were obtained. NH_2-MIL-53(Al) was synthesized using a modified procedure based on a previous report by Couck et al.[26] MIL-53(Al) was synthesized with the same composition as NH_2-MIL-53(Al) but using terephthalic acid rather than aminoterephthalic acid as a ligand. MIL-101(Cr) was synthesized using the molar composition previously reported by Khan et al.;[27] however, the synthesis was carried out in a microwave oven at 180 °C for 30 min. The reduction of temperature and time in comparison with the previously reported synthesis led to a decrease in particle size from 100 to 50 nm. The complete details for the syntheses of MOFs can be found in the Supporting Information.

Preparation of PI Supports. The cross-linked PI ultrafiltration (UF) support was prepared as follows: a 24% (w/w) polymer dope solution was prepared by dissolving PI (P84, HP Polymer GmbH) in dimethylformamide (DMF, HPLC grade, VWR International) and stirring overnight. A viscous solution (3582 cP at 25 °C) was formed and allowed to stand until the air bubbles disappeared. The dope solution was then cast on a polypropylene nonwoven backing material taped to a glass plate using a casting knife set at a thickness of 200 μm. The casting speed was 0.04 m$s^{−1}$ and the casting machine was located in a room at 20 °C. Immediately after casting, the membrane was immersed in a water bath (also at 20 °C), where phase inversion occurred. After 10 min, lengths of support were transferred to a fresh water bath (20 °C), left for 1 h, and then immersed in a solvent exchange bath [isopropyl alcohol (IPA), HPLC grade, VWR international] to remove any residual water or DMF. The supports were cross-linked via immersion in a solution of hexanediamine (HDA, 99.5%, Sigma Aldrich) in IPA (120 g/L) for 16 h at 20 °C. Next, each membrane was washed with IPA four times for 1 h to remove any residual HDA. Subsequently, these supports were conditioned with polyethylene glycol (PEG, MW 400, from VWR International) to avoid pore collapse as well as the formation of PA inside the pores during the IP reaction. The conditioning was carried out by immersing

the membranes in a bath comprising PEG/IPA at a volume ratio of 3:2 overnight. The membranes were then wiped dry with tissue paper.

Preparation of TFC and TFN−MOF Membranes. TFC PA membranes (without filler) were hand-cast on cross-linked PI P84 supports through interfacial polymerization. First, an aqueous solution of 2% (w/v) m-phenylenediamine (MPD, 99%, Sigma-Aldrich) and a solution of 0.1% (w/v) trimesoyl chloride (TMC, 98%, Sigma-Aldrich) in hexane (HPLC grade, VWR International) were prepared. The support was cut into disks of 60.8 cm^2 and placed in a glass filtration holder for the IP reaction. For this purpose, 15 mL of the aqueous solution was added and after 2 min the excess solution was removed and the membrane was wiped with tissue paper. Then, 15 mL of the hexane solution was poured and after 1 min reaction time the resulting membranes were withdrawn from the hexane solution and rinsed with water.

TFN−MOF membranes were prepared by following the same procedure as for TFC membranes, by dispersing typically 0.2% (w/v) of synthesized MOFs [ZIF-8, MIL-53(Al), NH$_2$-MIL-53(Al) and MIL-101(Cr)] in the organic phase before the IP reaction. Note that for TFN−MIL-101(Cr) membranes, the MOF concentration was varied from 0.05 to 0.4% (w/v). Nanoparticle dispersion was achieved by ultrasonication for 1 h at room temperature immediately prior to the IP reaction. Different post-treatments were carried out on TFC and TFN−ZIF-8 membranes to optimize the OSN performance, i.e. maximum flux and high rejection. Table 1 depicts five different post-treatments.

Table 1. Summary of Different Post-Treatments

code	post-treatment step
PT1	washing with 100 mL of water at 80 °C for 2 min
PT2	activation via dip coating with DMF for 20 min
PT3	washing with 100 mL of water at 80 °C for 2 min + DMF activation via dip coating
PT4	activation via filtration with DMF for 20 min
PT5	washing with 100 mL of water at 80 °C for 2 min + DMF activation via filtration for 20 min

treatments. TFN membranes with MIL-101(Cr), NH$_2$-MIL-53(Al), and MIL-53(Al) were treated via filtration with DMF (PT4), as explained in the Results and Discussion.

Characterization. Specific surface area measurements of ZIF-8 and MIL-101(Cr) were performed using a Micromeritics Tristar 3000 with N$_2$ at 77.4 K. Prior to the N$_2$ adsorption/desorption measurement, the samples were degassed under vacuum for 8 h at 200 °C. The specific surface area was calculated according to the BET (Brunauer−Emmett−Teller) method.

Powder XRD analyses were made using a D-Max Rigaku X-ray diffractometer with a copper anode and a graphite monochromator to select Cu Kα radiation (λ = 1.5418 Å).

Thermogravimetric analyses (TGA and DTG) were performed under air flow in a TGA/SDTA 851e system (Mettler Toledo) to study the water adsorption and thermal stability of the MOFs. The analyses were conducted from 25 up to 850 °C at a heating rate of 10 °C/min.

TFC/TFN membrane surfaces and MOF nanoparticles were characterized by scanning electron microscopy (SEM). SEM images were collected with a high-resolution field emission gun scanning electron microscope (Carl Zeiss Ltd.) operating at 5 kV. Samples were coated with chromium under an argon atmosphere in an Emitech K575X Peltier to ensure conductivity. For EDX analysis the samples were coated with gold and analyzed in an Inspect F scanning electron microscope. To verify the presence of MOFs in the TFN, membrane cross sectional and surface images were taken by transmission electron microscopy (TEM), with a Tecnai T20 operating at 200 kV. To obtain membrane cross sectional images, a lamella of the top 5 μm of the membrane was prepared using the focused ion beam (FIB) technique (Dual Beam 3 Nova 200), where the membrane, previously coated with platinum, was cut by accelerating concentrated gallium ions (30 KV, 50 pA) to a specific site. Once the lamella was created, it was lifted

out by a micromanipulator and glued on a support (carbon copper grid), where the final thinning (150 nm thickness) took place. For the membrane surface images, TFN−MIL-101(Cr) membranes were synthesized on an alumina support (20 nm pore size) instead of on cross-linked PI P84 support. The PA−MOF skin layer was detached from the support by floating on water and the film was placed on a carbon copper grid.

TFN−MIL-101(Cr) membrane surface composition (the top 60 nm) was analyzed using X-ray photoelectron spectroscopy (XPS). XPS was performed in an AXIS ultra DLD (Kratos Analytical) analysis system, using monochromated Al Kα (1486.6 eV) excitation at 12 kV and 10 mA. Prior to measurement, cleaned surface was obtained by spraying the sample with an ion beam of Ar$^+$ operating at 3 keV and with an emission current of 5 mA. To profile the concentration of MOF in the first nanometer layers, an etching ion gun was used (beam energy of 3 keV, 5 mA), taking data every hour. Data processing was performed using Casa XPS.

The wettability of the membranes was determined by contact angle analysis using a drop shape analyzer (DSA 10 MK2, Krüss) at 20 °C. The volume of the water droplets was 20 μL and at least five measurements were performed on each membrane sample. The samples were immersed in IPA and dried in air before the measurements.

ATR-FTIR was performed in a Bruker Vertex 70 spectrophotometer with a DTGS detector and Golden Gate accessory. The measurements were run from 600 to 4000 cm^{-1} with a resolution of 2 cm^{-1}.

Membrane Performance. Nanofiltration experiments were carried out in a pump pressurized cross-flow unit provided with eight cells connected in series. The performance of the membranes was evaluated by using two different solvents, tetrahydrofuran (THF, HPLC grade, VWR International) and methanol (MeOH, HPLC grade, VWR International), with kinetic diameters of 0.63 and 0.36 nm, respectively. Standard feed solutions comprising a homologous series of styrene oligomers (PS, 1 g·L^{-1} of PS580 and PS990, from Polymer Laboratories, and 0.01 g·L^{-1} of α-methylstyrene dimer, from Sigma-Aldrich) dissolved in the selected solvents were used for nanofiltration. Styrene oligomers were analyzed in the permeate and feed samples using an Agilent HPLC system with UV−vis detector set at a wavelength of 264 nm. All the experiments were carried out at 30 bar and a feed flow of 100 L·h^{-1}. The effective membrane area was 14 cm^2. Permeate samples for flux measurements were collected at intervals of 2 h, and samples for rejection evaluation were taken once steady state was reached (12 h). The MWCO (molecular weight cutoff) was determined by interpolating from the plot of rejection against molecular weight of the above-mentioned oligomers and corresponds to the molecular weight for which rejection is 90%.

Solvent flux (J) was determined by measuring permeate volume (V) per unit area (A) per unit time (t) according to the following eq 1:

$$J = \frac{V}{At} \tag{1}$$

The rejection (R_i) of markers was calculated from eq 2, where $C_{P,i}$ and $C_{F,i}$ correspond to marker concentrations in the permeate and the feed, respectively.

$$R_i = \left(1 - \frac{C_{P,i}}{C_{F,i}}\right) \times 100\% \tag{2}$$

■ RESULTS AND DISCUSSION

Characterization of MOFs. Figure 2 shows the SEM images of the MOFs that were synthesized and used as fillers for the preparation of TFNs: ZIF-8, NH$_2$-MIL-53(Al), MIL-53(Al), and MIL-101(Cr). All of them have nanometric crystal size and narrow particle size distribution.

N$_2$ adsorption measurements were carried out in order to determine the BET surface area of each sample. MOF
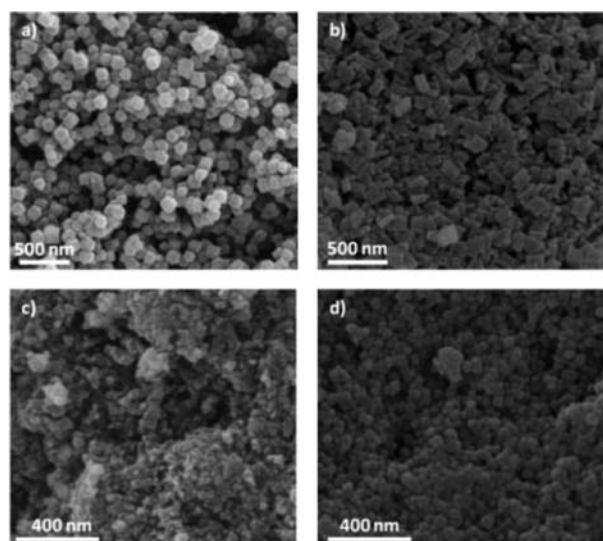
Figure 2. SEM images of (a) ZIF-8, (b) NH$_2$-MIL-53(Al), (c) MIL-53(Al), and (d) MIL-101(Cr).

structures were confirmed by X-ray diffraction and their thermal stability determined by TGA (Figures S1 and S2, Supporting Information). In addition, TGA analyses were performed after water adsorption experiments (Figure S3, Supporting Information) to estimate the amount of water adsorbed per gram of MOF. Table 2 summarizes all of these results.

Effect of Post-Treatments on the OSN Performance. In order to determine the most suitable post-treatment, PA TFC membranes without MOFs were prepared and subjected to the post-treatments described in the Experimental Section (Table 1). TFN membranes with ZIF-8 crystals were also synthesized and the same post-treatments followed. The OSN performance of TFCs and TFNs with these modifications was evaluated for MeOH/PS and THF/PS. The results obtained for the membranes are shown in Table S1 (Supporting Information). The rejection remained constant after hot water post-treatments, while the fluxes decreased slightly, possibly due to some tightening of the pores in the polyimide support membrane upon curing.[5] The post-treatment step via DMF dipping (PT2) and DMF filtration (PT4) enhanced solvent flux as a consequence of the removal of small molecular PA fragments. This effect has been previously observed and reported.[12] It has been explained by the swelling of the PA layer as DMF has a Hildebrand solubility parameter [23 (MPa)$^{1/2}$] similar to that of PA [24.8 (MPa)$^{1/2}$]. This improvement was larger when the DMF post-treatment was carried out by filtration instead of dipping. For both TFCs and TFNs the rejection was >90% in THF and MeOH for molecular weights ≥295 g·mol^{-1}. This proves that the thin film PA layer was also formed in the presence of ZIF-8 particles,

since the PI P84 support alone, i.e., without PA, prepared here gave rejections lower than 10%.[31] It also indicates that an intimate contact between the particles and the PA was achieved; i.e., the formation of nonselective voids was avoided. Since the MOFs are mixed with the TMC before reaction with the diamine, there might be a chance of chemical reaction of the MOFs with these reactants (in excess). In addition, once the PA film was formed, some interactions between the organic moieties of the filler and the carboxylic and amide groups in the PA could have taken place. In any case, these interactions would not affect the crystallinity of the MOFs, as will be proved later by TEM images, while explaining the close filler−polymer contact achieved.

This series of experiments was useful to set the optimum post-treatment, which was the activation via filtration with DMF for 20 min (post-treatment PT4 in Table 1). Hereafter, all the reported membranes were post-treated in this way.

Characterization of TFN−MOF Membranes. Table 3 shows the contact angle values for TFC and TFN membranes

Table 3. Contact Angle of TFC and TFN−MOF Membranes with 0.2% (w/v) Concentration in the Organic Phase before IP Reaction^a

membrane	contact angle (deg)^b			
TFC (without MOF)		73 ± 4		
TFN−NH$_2$-MIL-53(Al)		49 ± 2		
TFN−MIL-53(Al)		54 ± 5		
TFN−ZIF-8		75 ± 2		
TFN−MIL-101(Cr)	53 ± 1 (0.05)	52 ± 2 (0.1)	50 ± 4 (0.2)	43 ± 3 (0.4)

^{a}For TFN−MIL-101(Cr), concentration was changed from 0.05 to 0.4% (w/v). All the membranes were submitted to post-treatment PT4. ^{b}Values in parentheses correspond to % (w/v) MOF loading.

that contain MOFs with different hydrophobic/hydrophilic properties. When hydrophobic ZIF-8 particles were added, the contact angle slightly increased, and it decreased when hydrophilic NH$_2$-MIL-53(Al), MIL-53(Al), and MIL-101(Cr) nanoparticles were added. This decrease was more pronounced as the hydrophilic MOF loading increased. This result is consistent with the hydrophilic/hydrophobic properties of the embedded nanoparticles. A decrease in the contact angle after embedding hydrophilic nanoparticles was also observed in some previous works where mesoporous silica[14] and zeolite NaA[13] were embedded in polyamide TFN membranes. In these studies the changes in hydrophilicity were also attributed to possible changes in the chemical structure of the PA thin film formed in the presence of the nanoparticles, which may hydrate and release heat when in contact with MPD aqueous solution. In addition, the presence of hydrophilic MOFs may enhance the miscibility between the aqueous and organic phases during interfacial polymerization. If more acyl chloride groups in TMC remained on the surface without reacting, their hydrolysis could

Table 2. Textural Properties, Particle Size, and Water Adsorption Properties of the MOFs

MOF	pore/cavity diameter (nm)	BET surface area (m^2·g^{-1})	particle size (nm)	V_{pore} (cm^3·g^{-1})	water adsorption (g water/g MOF)
NH$_2$-MIL-53(Al)	0.75[28]	675[29]	133 ± 13	0.22[29]	0.7
MIL-53(Al)	0.86[28]	753[23]	60 ± 15	0.29[23]	1.3
ZIF-8	0.34/1.2[9]	1410	100 ± 10	0.76	0.1
MIL-101(Cr)	1.2/2.9[30] 1.6/3.4[30]	2306	47 ± 6	1.52	1.7

generate carboxylic acid groups therefore increasing surface hydrophilicity.[32]

Hereafter, TFN−MOF membrane characterization will focus on TFN−MIL-101(Cr) membranes, since they showed the best performance in OSN, as presented further. The ATR-FTIR spectra of cross-linked PI P84 support, TFC membrane, TFN−MIL-101(Cr) membranes at 0.2 and 0.4% (w/v), and MIL-101(Cr) powder are shown in Figure 3. The polyimide peaks at
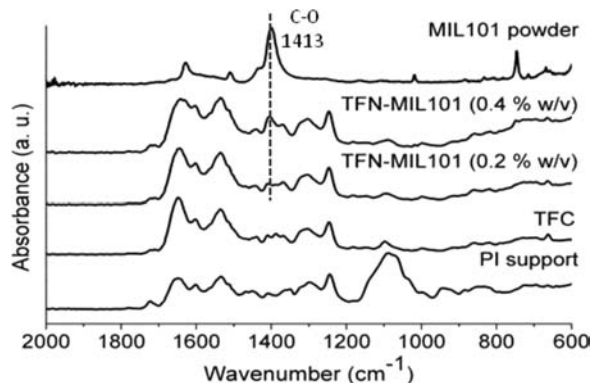

Figure 3. ATR-FTIR spectra of cross-linked PI P84 support, TFC membrane, TFN−MIL-101 membranes at 0.2 and 0.4% (wt/v), and MIL-101(Cr) powder.

1378 and 1731 cm^{-1} in the spectrum of cross-linked PI P84 support correspond to C−N and C=O bonds, respectively, and are weaker in the TFC spectrum. Peaks at 1655 cm^{-1} (amide I, C=O stretching vibrations of amide), 1545 cm^{-1} (amide II, in-plane N−H bending and C−N stretching vibrations), and 1467 and 1415 cm^{-1} (these last two corresponding to amide functionalities) are related to the PA layer formed upon interfacial polymerization.[12,14] TFN−MIL-101(Cr) membranes showed the same peaks, which means that the PA layer was formed in the presence of MOF nanoparticles. In addition, a new peak at 1413 cm^{-1} appears in the spectra of TFN−MIL-101(Cr) membranes, whose intensity increased with MOF loading. This peak is attributed to the C−O bond of the C−OH group of carboxylic acid and confirmed the presence of MOF nanoparticles in the PA thin layer.

Parts a and b of Figure 4 respectively show SEM images of TFC and TFN−MIL-101(Cr) [0.2% (w/v)] membrane surfaces after DMF treatment (PT2; see Table 1). The membrane surface became smoother after DMF treatment (Figure S4, Supporting Information) due to partial surface etching. Part of the loose PA structure was dissolved, removing oligomers of smaller molecular weights, as previously reported.[12,33] In TFN−MIL-101(Cr) membranes, small aggregates of nanoparticles with the same spherical shape and particle size as MIL-101(Cr) crystals were observed on the membrane surface (black circles in Figure 4b). To confirm that these particles were MOFs rather than PA molecular fragments, EDX analyses were carried out on the PA layer, where the chromium present in the MIL-101(Cr) framework was detected (see Figure S5 and Table S2, Supporting Information). Figure 4c shows a TEM image of the TFN−MIL-101(Cr) cross-section lamella. The black part corresponds to the platinum coating done in FIB to protect the membrane surface from the gallium ions. An amplification of this area (Figure 4c, inset) shows the PA−MOF layer protruding from the PI P84 support, with a thickness of 54 ± 10 nm. The
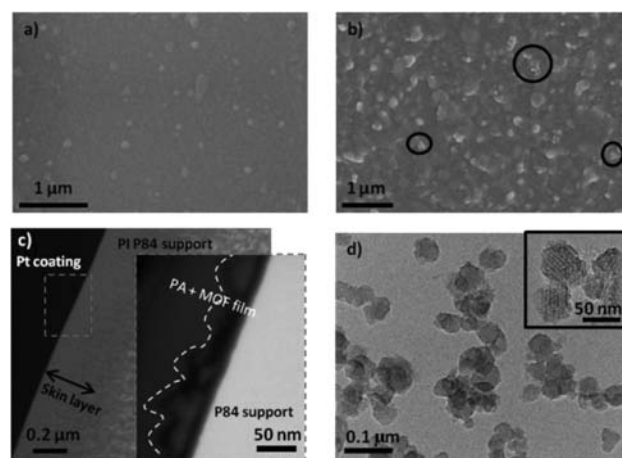

Figure 4. (a) SEM image of TFC membrane surface after DMF dipping, (b) SEM image of TFN−MIL-101(Cr) [0.2% (w/v)] membrane surface after DMF dipping, (c) TEM image of TFN−MIL-101(Cr) [0.2% (w/v)] cross-section membrane lamella prepared using the FIB technique. (d) TEM image of detached PA−MIL-101(Cr) thin film surface, where the inset is at a higher magnification.

contrast difference across the PI P84 support image (Figure 4c) suggests that the skin layer thickness of the PI P84 support is about 200 nm, which is in agreement with the literature.[34] TEM images of PA-MIL-101(Cr) thin film surface (Figure 4d) confirmed the crystalline structure of MIL-101(Cr) particles embedded in the PA layer after IP reaction, where the dark contrast lines related to the pores are observed in the inset.[11]

The amount of Cr was estimated by XPS chemical analysis on the TFN−MIL-101(Cr) 0.2% (w/v) membrane. An average composition of 1.6 ± 0.1 wt % Cr was calculated from three measurements, starting from the top of the membrane at 30 nm thickness intervals (i.e., in 60 nm total thickness). According to the MIL-101(Cr) formula [$Cr_3O(OH)(H_2O)_2[C_6H_4(CO_2)_2]_3$·$25H_2O$], which coincides with the chemical analysis of MIL-101 powder, this percentage corresponds to 12 ± 1 wt % MIL-101 particles in the top PA layer. This MOF concentration inside the layer depends on the percentage of MOF added in the TMC−hexane solution prior IP and is directly correlated to the solvent flux increase, as will be shown below.

OSN Results for TFN−MOF Membranes. Table 4 shows the MeOH and MeOH/PS permeances obtained for the TFC and TFN membranes using different MOFs with a loading of 0.2% (w/v) in the organic phase prior to the IP reaction. The membranes were reproducible with relatively small errors (obtained averaging the performance of three or four different membranes) in the permeance values, and the rejection was

Table 4. OSN Results of TFN Membranes for MeOH, at 30 °C and 30 bar[a]

	permeance (L·m^{-2}·h^{-1}·bar^{-1})	
membrane	MeOH	MeOH/PS
TFC (without MOF)	1.8 ± 0.2	1.5 ± 0.1
TFN− NH$_2$-MIL-53(Al)	2.3 ± 0.2	1.8 ± 0.3
TFN−MIL-53(Al)	2.3 ± 0.4	1.9 ± 0.3
TFN−ZIF-8	2.5 ± 0.6	2.1 ± 0.3
TFN−MIL-101(Cr)	4.2 ± 0.1	3.9 ± 0.3

[a]The values given are an average of three or four different membranes. All the membranes were submitted to post-treatment PT4.

>90% for all the TFN−MOF membranes (Figure 5). Note that pure MeOH permeance was slightly higher than that of MeOH
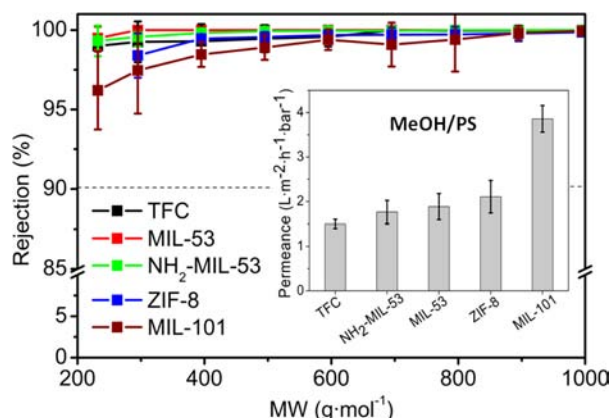

Figure 5. MWCO curves of TFN−MOF membranes submitted to post-treatment PT4 for MeOH/PS solution nanofiltration. Inset: MeOH/PS permeance of TFC and TFN−MOFs membranes. Nanofiltration experiments were performed at 30 °C and 30 bar.

permeance in the MeOH/PS system, for all the membranes. This is most likely due to a combination of the concentration polarization effect, i.e., the accumulation of rejected PS in a boundary layer at the membrane surface, and some surface and pore fouling by the PS.

The bulk fluid feed concentration is used to calculate the apparent rejection reported in this work. Concentration polarization causes this apparent rejection value to be lower than the true rejection of the membrane, which would be calculated using the solute concentration on the membrane surface. However, the mass transfer coefficient in our system was previously reported to be 5.3×10^{-5} m·s^{-1} for solute concentrations in the same range,[35] which is high enough that the apparent and true rejections will be close.

TFN membranes with microporous MOFs [ZIF-8, NH$_2$-MIL-53(Al) and MIL-53(Al)] led to higher MeOH fluxes and similar rejections as the TFC membranes without MOFs (>90%). However, a tremendous enhancement of the membrane performance was obtained when mesoporous MIL-101(Cr) particles were embedded into the PA layer. The rejection of PS remained >90% while the permeance of MeOH increased from 1.5 to 3.9 L·m^{-2}·h^{-1}·bar^{-1} (160%). This increase in permeance can be related to the porosity of each MOF. Figure 5 (inset) represents the MeOH/PS permeance of TFC and TFN−MOF membranes, where it can be seen that as the pore size and porosity (BET area and pore volume; see Table 2) of the added MOF increase [NH$_2$-MIL-53(Al) < MIL-53(Al) < ZIF-8 < MIL-101(Cr)], so too does the permeance.

In these TFN−MOF membranes we believe that the high rejection is due to the selective PA layer surrounding the MOF nanoparticles. The excellent compatibility between the PA and the MOF particles eliminates the formation of nonselective voids. The increase in fluxes is related to the porosity of the MOFs, which provides preferential flow paths for the solvents. When compared with the TFN containing microporous MOFs, the mesoporous MOF MIL-101(Cr), with the largest pore size (1.6/3.4 nm; see Table 2) and highest BET specific surface area (2306 m^2·g^{-1}), showed the highest enhancement in permeance. These remarkable permeances suggest that the short flow paths through the hydrophilic porous structure of MIL-101(Cr)

nanoparticles play an important role in MeOH permeation. In addition to the high porosity, the degree of cross-linking in the PA film could change in the presence of the MOF nanoparticles. An analogous enhancement in permeation has been observed when hydrophilic MCM-41 silica has been added into the PA thin film layer, resulting in an increase in the permeate water flux from 28.5 to 46.6 L·m^{-2}·h^{-1} with a salt rejection of 97.9%.[14]

The significant improvement in the OSN performance of TFN−MIL-101(Cr) membranes led us to test them without DMF post-treatments (Table S3, Supporting Information). It was found that for these membranes DMF filtration was a key step, since MeOH and THF permeances were much lower before DMF treatment. However, TFN−MIL-101(Cr) membranes always led to higher fluxes in comparison with the same post-treated TFC membranes, illustrating clearly the benefits of the presence of the high porosity filler inside the PA thin layer.

OSN Results for TFN−MIL-101(Cr) Membranes with Increasing MOF Loadings. To study the effect of increasing MOF loading on the permeation and rejection, TFN−MIL-101(Cr) membranes with 0.05−0.4% (w/v) nanoparticles loading were prepared and tested in MeOH and THF nanofiltration experiments. All the membranes were treated with DMF (PT4) before OSN experiments. Figure 6 shows the
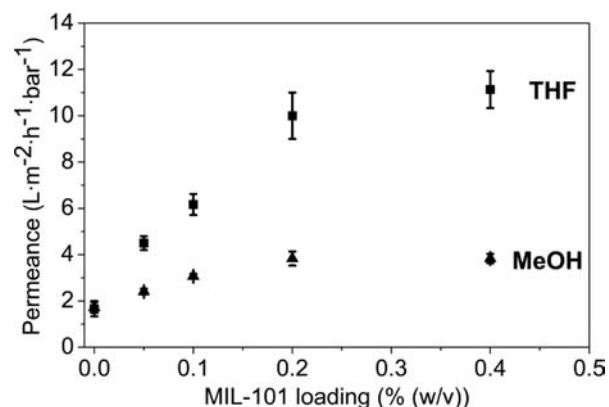

Figure 6. MeOH/PS and THF/PS permeances at different MIL-101(Cr) loadings in the organic phase before the IP reaction. The experiments were carried out at 30 °C and 30 bar. The standard deviations were calculated from an average of two or three membranes.

THF/PS and MeOH/PS permeances and Figure 7 the rejections obtained at different loadings, all at 30 °C and 30 bar. It is of note that the MeOH/PS and THF/PS performances obtained for bare TFC (without MOF) are in agreement with previously reported data (i.e., 1.5 L·m^{-2}·h^{-1}·bar^{-1} for MeOH/PS and 1.7 L·m^{-2}·h^{-1}·bar^{-1} for THF/PS).[12]

The THF and MeOH permeances increased almost linearly with the MIL-101(Cr) loading up to 0.2% (w/v), since MOF pores open the path for the solvent molecules. However, the loading increment from 0.2 to 0.4% (w/v) led to only a slight increase in permeance. This result could be due to the aggregation of MIL-101(Cr) particles at high concentrations, which would hinder good dispersion and consequently access to the MOF pores.[14,36] The rejection did not depend on the MOF loading, since no trend is evident in Figure 7. The MWCO remained less than 232 g·mol^{-1} in MeOH and at 295 g·mol^{-1} in THF for all loadings. For TFN−MIL-101(Cr) 0.2% (w/v), MeOH/PS permeance increased 160% in comparison with bare TFC membranes without MOF, up to 3.9 L·m^{-2}·h^{-1}·
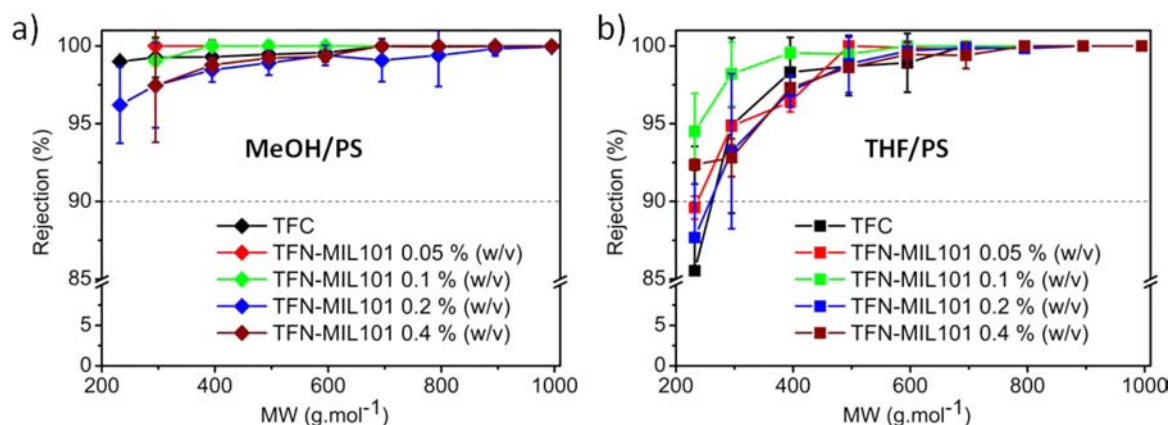
Figure 7. MeOH/PS (left) and THF/PS (right) rejections at different MIL-101(Cr) loadings. The experiments were carried out at 30 °C and 30 bar. The standard deviations were calculated from an average of two or three membranes.

bar^{-1}, whereas for THF/PS solution the increment was 488%, up to 10.0 L·m^{-2}·h^{-1}·bar^{-1}. For THF/PS permeance, the highest value was obtained with TFN−MIL-101(Cr) 0.4% (w/v), for which a permeance of 11.1 L·m^{-2}·h^{-1}·bar^{-1} was obtained with a rejection >90%. The fact that THF fluxes increased to a greater extent than MeOH fluxes with the addition of MOF can be explained by considering the properties of each solvent. THF has lower viscosity than MeOH. In addition, the dielectric constant of MeOH (33.6) is higher than that of THF (7.6). Since MeOH is more hydrophilic, it is likely that the interaction of this solvent with the hydrophilic MOF MIL-101(Cr) is stronger than the interaction of this MOF with THF. Therefore, THF is more weakly adsorbed in the pores of MIL-101(Cr), and the resulting diffusion through the membrane is faster. In comparison with the results obtained for commercial integrally skinned asymmetric OSN membranes (DuraMem DM150 from Evonik MET Ltd., UK),[12] measured in the same experimental setup, TFN−MIL-101(Cr) 0.2% (w/v) membranes increased the THF/PS permeance up to 100 times, i.e., from 0.1 (commercial membrane DM150) to 10.0 L·m^{-2}·h^{-1}·bar^{-1}. This shows the huge potential of nanosized, highly porous MOFs to improve the transport properties of TFC membranes for OSN through provision of structured, porous regions in the thin film.

CONCLUSIONS

The formation of thin film nanocomposite membranes (TFN) by embedding MOFs in a thin polyamide layer (supported on a stable cross-linked polyimide) via interfacial polymerization has been demonstrated. These membranes combine the benefits of MOFs (nanosize, tunable porosity, flexible structure, and chemical composition) with the easy processability of thin film composite membranes.

TFN membranes tested in MeOH/PS and THF/PS nanofiltration experiments showed dramatically increased permeance when compared to the same membranes with no MOFs, without sacrificing rejection. A direct trend was observed between the MeOH/PS permeance and the porosity properties of the MOFs added to the thin film layer. This result suggests that the increase in flux was due to the porosity of the MOFs, which provided preferential flow paths for the solvents. The high rejection was achieved by the polyamide layer surrounding the nanoparticles and by the good compatibility between the polyamide and the organic moieties of the MOF particles.

The membrane permeance increased with MOF loading in the TFN membranes, while keeping high rejections. The best performance was observed when mesoporous MIL-101(Cr) was used, with flux increases from 1.5 to 3.9 and from 1.7 to 11.1 L·m^{-2}·h^{-1}·bar^{-1} for MeOH/PS and THF/PS mixtures, respectively.

These novel MOF-TFN membranes suggest a new generation of high performance organic solvent nanofiltration membranes, in which loading the PA thin film separating layer with small amounts of MOFs can remarkably increase flux while preserving rejection. Moreover, tunable membranes could be developed by combining microporous and mesoporous MOFs within a single thin film.

■ ASSOCIATED CONTENT

ⓢ Supporting Information

Synthesis procedure and characterization of MOFs (XRD, TGA), OSN results of TFC and TFN−ZIF-8 membranes with different post-treatments, characterization of TFC/TFN membranes (EDX, SEM), and OSN results of TFN−MIL-101(Cr) membranes with different post-treatments. This material is available free of charge via the Internet at http://pubs.acs.org.

■ AUTHOR INFORMATION

Corresponding Author

a.livingston@imperial.ac.uk; coronas@unizar.es

Present Address

§The School of Materials, The University of Manchester, Oxford Road, Manchester M13 9PL, U.K.

Author Contributions

All authors have given approval to the final version of the manuscript.

Notes

The authors declare no competing financial interest.

■ ACKNOWLEDGMENTS

■ REFERENCES

(1) Vandezande, P.; Gevers, L. E. M.; Vankelecom, I. F. J. *Chem. Soc. Rev.* **2008**, *37*, 365−405.

(2) Razdan, U.; Joshi, S. V.; Shah, V. J. *Curr. Sci.* **2003**, *85*, 761−771.

(3) Petersen, R. J. *J. Membr. Sci.* **1993**, *83*, 81−150.

(4) See-Toh, Y. H.; Lim, F. W.; Livingston, A. G. *J. Membr. Sci.* **2007**, *301*, 3−10.

(5) See-Toh, Y. H.; Ferreira, F. C.; Livingston, A. G. *J. Membr. Sci.* **2007**, *299*, 236−250.

(6) Park, H. B.; Lee, C. H.; Sohn, J. Y.; Lee, Y. M.; Freeman, B. D.; Kim, H. *J. Membr. Sci.* **2006**, *285*, 432−443.

(7) Lin, A. A.; Sastri, V. R.; Tesoro, G.; Reiser, A.; Eachus, R. *Macromolecules* **1988**, *21*, 1165−1169.

(8) Tin, P. S.; Chung, T. S.; Liu, Y.; Wang, R.; Liu, S. L.; Pramoda, K. P. *J. Membr. Sci.* **2003**, *225*, 77−90.

(9) Park, K. S.; Ni, Z.; Cote, A. P.; Choi, J. Y.; Huang, R. D.; Uribe-Romo, F. J.; Chae, H. K.; O'Keeffe, M.; Yaghi, O. M. *Proc. Natl. Acad. Sci. U. S. A.* **2006**, *103*, 10186−10191.

(10) Chin, J. M.; Chen, E. Y.; Menon, A. G.; Tan, H. Y.; Hor, A. T. S.; Schreyer, M. K.; Xu, J. *CrystEngComm* **2013**, *15*, 654−657.

(11) Lebedev, O. I.; Millange, F.; Serre, C.; Van Tendeloo, G.; Ferey, G. *Chem. Mater.* **2005**, *17*, 6525−6527.

(12) Jimenez-Solomon, M. F.; Bhole, Y.; Livingston, A. G. *J. Membr. Sci.* **2012**, *423*, 371−382.

(13) Jeong, B.-H.; Hoek, E. M. V.; Yan, Y.; Subramani, A.; Huang, X.; Hurwitz, G.; Ghosh, A. K.; Jawor, A. *J. Membr. Sci.* **2007**, *294*, 1−7.

(14) Yin, J.; Kim, E.-S.; Yang, J.; Deng, B. *J. Membr. Sci.* **2012**, *423*, 238−246.

(15) Bao, M.; Zhu, G.; Wang, L.; Wang, M.; Gao, C. *Desalination* **2013**, *309*, 261−266.

(16) Lee, H. S.; Im, S. J.; Kim, J. H.; Kim, H. J.; Kim, J. P.; Min, B. R. *Desalination* **2008**, *219*, 48−56.

(17) Zacher, D.; Shekhah, O.; Woell, C.; Fischer, R. A. *Chem. Soc. Rev.* **2009**, *38*, 1418−1429.

(18) Zornoza, B.; Tellez, C.; Coronas, J.; Gascon, J.; Kapteijn, F. *Microporous Mesoporous Mater.* **2013**, *166*, 67−78.

(19) Bux, H.; Liang, F.; Li, Y.; Cravillon, J.; Wiebcke, M.; Caro, J. *J. Am. Chem. Soc.* **2009**, *131*, 16000−16001.

(20) Tanh Jeazet, H. B.; Staudt, C.; Janiak, C. *Dalton Trans.* **2012**, *41*, 14003−27.

(21) Liu, X. L.; Li, Y. S.; Zhu, G. Q.; Ban, Y. J.; Xu, L. Y.; Yang, W. S. *Angew. Chem., Int. Ed.* **2011**, *50*, 10636−10639.

(22) Shi, G. M.; Yang, T.; Chung, T. S. *J. Membr. Sci.* **2012**, *415*, 577−586.

(23) Basu, S.; Maes, M.; Cano-Odena, A.; Alaerts, L.; De Vos, D. E.; Vankelecom, I. F. J. *J. Membr. Sci.* **2009**, *344*, 190−198.

(24) Lind, M. L.; Ghosh, A. K.; Jawor, A.; Huang, X.; Hou, W.; Yang, Y.; Hoek, E. M. V. *Langmuir* **2009**, *25*, 10139−10145.

(25) Venna, S. R.; Carreon, M. A. *J. Am. Chem. Soc.* **2010**, *132*, 76−78.

(26) Couck, S.; Denayer, J. F. M.; Baron, G. V.; Remy, T.; Gascon, J.; Kapteijn, F. *J. Am. Chem. Soc.* **2009**, *131*, 6326−6327.

(27) Khan, N. A.; Kang, I. J.; Seok, H. Y.; Jhung, S. H. *Chem. Eng. J.* **2011**, *166*, 1152−1157.

(28) Boutin, A.; Couck, S.; Coudert, F. X.; Serra-Crespo, P.; Gascon, J.; Kapteijn, F.; Fuchs, A. H.; Denayer, J. F. M. *Microporous Mesoporous Mater.* **2011**, *140*, 108−113.

(29) Gascon, J.; Aktay, U.; Hernandez-Alonso, M. D.; van Klink, G. P. M.; Kapteijn, F. *J. Catal.* **2009**, *261*, 75−87.

(30) Ferey, G.; Mellot-Draznieks, C.; Serre, C.; Millange, F.; Dutour, J.; Surble, S.; Margiolaki, I. *Science* **2005**, *309*, 2040−2042.

(31) Soroko, I.; Makowski, M.; Spill, F.; Livingston, A. *J. Membr. Sci.* **2011**, *381*, 163−171.

(32) Kim, C. K.; Kim, J. H.; Roh, I. J.; Kim, J. J. *J. Membr. Sci.* **2000**, *165*, 189−199.

(33) Aharoni, S. M. *J. Appl. Polym. Sci.* **1992**, *45*, 813−817.

(34) Stawikowska, J.; Livingston, A. G. *J. Membr. Sci.* **2012**, *413*, 1−16.

(35) Peeva, L. G.; Gibbins, E.; Luthra, S. S.; White, L. S.; Stateva, R. P.; Livingston, A. G. *J. Membr. Sci.* **2004**, *236*, 121−136.

(36) Kim, E.-S.; Deng, B. *J. Membr. Sci.* **2011**, *375*, 46−54.